Versatile strategy for controlling the specificity and activity of engineered T cells

Jennifer S. Y. Ma[a,1], Ji Young Kim[a], Stephanie A. Kazane[a,2], Sei-hyun Choi[b], Hwa Young Yun[b,3], Min Soo Kim[a,4], David T. Rodgers[a], Holly M. Pugh[a], Oded Singer[a], Sophie B. Sun[a], Bryan R. Fonslow[c,d], James N. Kochenderfer[e], Timothy M. Wright[a], Peter G. Schultz[a,b,5], Travis S. Young[a,5], Chan Hyuk Kim[a,5], and Yu Cao[b,1]

[a]Department of Biology, California Institute for Biomedical Research, La Jolla, CA 92037; [b]Department of Chemistry and The Skaggs Institute for Chemical Biology, The Scripps Research Institute, La Jolla, CA 92037; [c]Department of Chemical Physiology, The Scripps Research Institute, La Jolla, CA 92037; [d]SCIEX Separations, Brea, CA 92821; and [e]Experimental Transplantation and Immunology Branch, National Institutes of Health, National Cancer Institute, Bethesda, MD 20892

Contributed by Peter G. Schultz, December 10, 2015 (sent for review October 23, 2015; reviewed by Carl H. June and Kevan M. Shokat)

The adoptive transfer of autologous T cells engineered to express a chimeric antigen receptor (CAR) has emerged as a promising cancer therapy. Despite impressive clinical efficacy, the general application of current CAR–T-cell therapy is limited by serious treatment-related toxicities. One approach to improve the safety of CAR-T cells involves making their activation and proliferation dependent upon adaptor molecules that mediate formation of the immunological synapse between the target cancer cell and T-cell. Here, we describe the design and synthesis of structurally defined semisynthetic adaptors we refer to as "switch" molecules, in which anti-CD19 and anti-CD22 antibody fragments are site-specifically modified with FITC using genetically encoded noncanonical amino acids. This approach allows the precise control over the geometry and stoichiometry of complex formation between CD19- or CD22-expressing cancer cells and a "universal" anti-FITC–directed CAR-T cell. Optimization of this CAR–switch combination results in potent, dose-dependent in vivo antitumor activity in xenograft models. The advantage of being able to titrate CAR–T-cell in vivo activity was further evidenced by reduced in vivo toxicity and the elimination of persistent B-cell aplasia in immune-competent mice. The ability to control CAR-T cell and cancer cell interactions using intermediate switch molecules may expand the scope of engineered T-cell therapy to solid tumors, as well as indications beyond cancer therapy.

cancer immunotherapy | chimeric antigen receptor T cell | noncanonical amino acids | cytokine release syndrome | B-cell aplasia

Second-generation CD19-targeting chimeric antigen receptor (CAR) T cells engineered with costimulatory signaling domains have generated potent antileukemic responses in patients with refractory B-cell malignancies (1–3). In light of their clinical promise, there has been an explosion of interest in CAR-T cells for cancer therapy, especially for the treatment of relapsed, refractory malignancies. However, current CAR–T-cell therapy is associated with serious treatment-related toxicities resulting from the uncontrollable release of cytokines (cytokine release syndrome, CRS) from synchronously activated and rapidly proliferating CAR-T cells. CRS is currently managed with anti–IL-6 receptor antibodies or by suppressing CAR–T-cell activity with corticosteroids (4, 5). In addition, the "on-target, off-tumor" activity of CD19-specific CAR-T cells results in the long-term depletion of B-cells in patients, which can be managed with Ig replacement therapy (2, 6, 7). This latter example of normal tissue toxicity is more problematic when targeting solid tumor-associated antigens (TAAs), where antigen expression is generally less restricted than hematologic markers (5, 8–11).

To minimize treatment-related toxicities yet retain potent antitumor activity, several strategies have been developed to regulate the persistence or enhance tumor selectivity of CAR–T-cell therapy. Suicide genes and transient mRNA CAR have been used to induce T-cell apoptosis and shorten the lifespan of these potent CAR-T cells, respectively (12, 13). To improve CAR–T-cell selectivity for tumor cells, dual targeting CARs that require the engagement of two TAAs to induce full activation and proliferation of CAR-T cells have been described (14). Another approach is the use of inhibitory CARs, which bind to antigens found on normal cells and result in the inhibition of CAR–T-cell function (15). Recently, Wu et al. described an approach using a small molecule to induce the assembly of a functional CAR complex, and thus control CAR–T-cell activity (16). Alternatively, it has been shown that CAR–T-cell activity can be controlled using soluble intermediary "switch" molecules. These switches are comprised of a tumor-targeting antibody or small-molecule ligand and a second moiety that selectively binds the CAR and not an endogenous receptor. CAR–T-cell activity is thus strictly dependent on the formation of a ternary complex between the CAR-T cell, switch, and tumor antigen. Therefore, titration or removal of the switch molecule can control or terminate CAR–T-cell response, respectively. Notably, unlike the suicide-gene approach described above, these switchable CAR-T cells are expected to remain in patients after

Significance

Despite the unprecedented antileukemic response demonstrated in recent clinical trials, the inability to control the potent chimeric antigen receptor (CAR)—T-cell activity has resulted in several serious adverse incidents. Herein, we demonstrate that a switch-mediated CAR-T approach enables the titration of engineered T-cell antitumor activity, which was observed to be highly advantageous in reducing treatment-related toxicities in vivo. Moreover, we show that the use of optimized antibody-based switches readily enables a single CAR construct to target different antigens, indicating its potential application to treat tumor escape variants and heterogeneous tumors expressing distinct tumor antigens. Our data support the safe application of this potent immune cell-based therapy to target other types of cancer, including solid tumors, as well as nononcology indications.

Author contributions: J.S.Y.M., J.Y.K., T.M.W., P.G.S., T.S.Y., C.H.K., and Y.C. designed research J.S.Y.M., J.Y.K., M.S.K., D.T.R., O.S., and Y.C. performed research; S.A.K., S.-h.C., H.Y.Y., H.M.P., S.B.S., B.R.F., and J.N.K. contributed new reagents/analytic tools; P.G.S., T.S.Y., and C.H.K. analyzed data; and J.S.Y.M., P.G.S., and C.H.K. wrote the paper.

Reviewers: C.H.J., University of Pennsylvania; and K.M.S., University of California, San Francisco.

The authors declare no conflict of interest.

Freely available online through the PNAS open access option.

[1]J.S.Y.M. and Y.C. contributed equally to this work.

[2]Present address: Protein Chemistry Department at Centers for Therapeutic Innovation, Pfizer, Inc., San Diego, CA 92121.

[3]Present address: College of Pharmacy, Pusan National University, Geumjeonggu, Busan 609–735, Korea.

[4]Present address: Department of Research and Development, Sorrento Therapeutics, Inc., San Diego, CA 92121.

[5]To whom correspondence may be addressed. Email: schultz@scripps.edu, tyoung@calibr.org, or chkim@calibr.org.

This article contains supporting information online at www.pnas.org/lookup/suppl/doi:10.1073/pnas.1524193113/-/DCSupplemental.

termination of treatment, which may be beneficial in incidences that require further treatments. In addition, unlike the intracellular switch approach described by Wu et al., an intercellular switch approach enables the targeting of multiple TAAs with a "universal" CAR-T cell. Examples of switches used in this approach include TAA-specific monoclonal antibodies that elicit antitumor activity from Fc-specific CAR-T cells (17), and chemically or enzymatically modified antibody–hapten conjugates that redirect antihapten CAR-T cells (18, 19). Recently, we have demonstrated the redirection of anti-FITC CAR-T cells with a heterobifunctional small-molecule switch, folate-FITC, which selectively targets folate receptor-overexpressing cancers (20). Although these reports established the feasibility of eliciting an anticancer response with switchable CAR-T (sCAR-T) cells, it has yet to be shown whether the efficacy of sCAR-T cells is comparable to current CAR-T cell therapies in the clinic.

Another limitation of conventional CAR–T-cell therapy is the inability of a single CAR-T cell to target multiple TAAs. For example, a second engineered CAR-T cell is required to target the outgrowth of resistant cancer cells lacking the original surface antigen target, or heterogeneous tumor populations expressing distinct TAAs. Moreover, recent studies have demonstrated the need to engineer the single-chain variable fragments (scFv) and the spacer region within the CAR structure for optimal efficacy (12, 21, 22). Therefore, generation of a universal CAR-T cell that can be readily endowed with multiple TAA specificities is highly desirable to minimize the risk for developing escape variants, and to simplify the clinical implementation of CAR–T-cell therapy.

Herein, we describe the development of antibody-based switches with site-specific conjugation of an FITC tag that enable the rapid optimization of a productive pseudoimmunological synapse between anti-FITC CAR-T cells and a given TAA. We demonstrate potent antigen-specific and dose-dependent in vitro and in vivo efficacies of these sCAR-T cells against CD19-expressing cancer cell lines. More importantly, we demonstrate that the strict dependence of CAR–T-cell activity on switch concentration can be exploited to enhance the in vivo safety (severe CRS and long-term B-cell depletion) associated with CAR–T-cell therapies. Finally, using two clinically validated B-cell markers, CD19 and CD22, we establish that this approach can be used to rapidly optimize different antigen-specific switch intermediates, which should allow one to target distinct TAAs with a single CAR construct.

Results

Design and Synthesis of sCAR-T Cells and Switch Molecules. To redirect the specificity of CAR-T cells with a switch molecule, we first generated CAR-T cells that bind the synthetic dye, fluorescein (FITC), which is physiologically absent and has demonstrated excellent selectivity in imaging agents and in antibody or small-molecule–based switch designs (18, 20, 23). We generated CAR-T cells using a range of anti-FITC scFv sequences that differ in their affinities toward FITC (24–27), and found that all anti-FITC CAR-T cells elicit in vitro cytotoxicity with the same switch (*vide infra*) to a similar extent (*SI Appendix*, Fig. S1*A*). Therefore, we chose the fully human FITC-E2 scFv (27) sequence for our anti-FITC CAR because it is expected to minimize the potential for immunogenicity (28). FITC-E2 scFv was inserted into a second-generation CAR expression cassette in a lentiviral vector that encodes the hinge and transmembrane region of the human CD8 followed by the cytoplasmic domains of human 4-1BB and CD3ζ (29) (*SI Appendix*, Fig. S1*B*). Viral particles were produced and used to transduce activated human peripheral blood mononuclear cells, as previously described (20). Seven days postviral transduction, CAR expression varied from ∼40–60% as determined by flow cytometry using APC-labeled anti-human IgG and FITC-conjugated isotype antibody (*SI Appendix*, Fig. S1*C*).

As our initial sCAR-T target, we chose CD19, an antigen that is highly expressed on B-cell cancers. For the switch itself, we used the anti-CD19–specific monoclonal antibody, clone FMC63, which was previously used in a second-generation CAR-T cells against B-cell cancers (1, 30, 31). The Fab format was chosen over full-length IgG because of its shorter half-life (32), which allows for better temporal control of CAR–T-cell activity. To study the effect of the FITC conjugation site on the distance and geometry of the pseudoimmunological synapse formed between CAR, TAA, and switch, we used a site-specific protein conjugation strategy (33). This approach has been similarly used to optimize the geometry and pharmacology of antibody drug conjugates and bispecific antibodies (34–36). This method involves the genetic incorporation of noncanonical amino acids with bio-orthogonal chemical reactivity at defined positions in an antibody to generate chemically defined small-molecule conjugates (33, 36, 37). Specifically, the noncanonical amino acid para-azidophenylalanine (pAzF) was incorporated individually at six surface-exposed positions (A, G68; B, S74; C, T109; D, A121; E, S202; and F, K138) based on the crystal structure of a murine Fab 93f3 (PDB ID code 1T4K) (Fig. 1*A*). The distinct location of each conjugation site relative to the antigen-binding region (proximal A and B; medial C and D; distal E and F) in the anti-CD19 Fab is expected to afford geometrically distinct immunological synapses. In addition to monovalent conjugates, we also generated bivalent FITC conjugates, AB and EF, to determine the effect of valency on CAR–T-cell activity.

To express mutant Fabs, a plasmid encoding the FMC63 gene with an amber (TAG) codon at the desired position was cotransformed into *Escherichia coli* with a plasmid harboring an orthogonal amber suppressor tRNA/aminoacyl-tRNA synthetase pair that was evolved to incorporate pAzF in response to the TAG codon. The purified Fabs were subsequently conjugated with an FITC linker with a terminal cyclooctyne group to allow for selective coupling to pAzF via a "click" reaction under neutral pH (PBS, pH 7.4) (*SI Appendix*, Fig. S2*A*). The molecular weight and purity of each construct was analyzed by SDS/PAGE and mass spectrometry (MS), which confirmed that homogenous reaction products with a conjugation efficiency of >95% were generated (*SI Appendix*, Fig. S2*B*). For comparison, we also generated a random FITC conjugate using *N*-hydroxysuccinimide (NHS) chemistry, which yielded an average FITC to antibody ratio of 2 (*SI Appendix*, Fig. S3 *A* and *B*). MS analysis after tryptic digestion revealed ∼58% of the conjugates were modified at the heavy-chain N-terminal amino group and the remaining conjugation occurred at lysine residues within the light chain, largely at K31 (∼20%) and K141 (∼68.4%) (*SI Appendix*, Fig. S3 *C*–*E*). Next, we assessed the binding of FITC-labeled anti-CD19 switches by flow cytometry. As shown in *SI Appendix*, Fig. S4*A*, the binding affinities of all site-specific FITC switches to $CD19^+$ target cells (Nalm-6) were comparable to the parental anti-CD19 Fab (0.4–1.6 nM), whereas slightly decreased binding was observed with the random conjugate (EC_{50} = 4.0 nM), a likely consequence of modification within the CDR1 of light chain at position K31 (Fig. 1*A*). No binding was observed with $CD19^-$ cells (K562) (*SI Appendix*, Fig. S4*B*). Bivalent FITC conjugates (EC_{50} = ∼3 nM) exhibited two- to threefold higher affinity for the anti-FITC CAR-T cells than monovalent FITC switches (EC_{50} = 6–9 nM) (*SI Appendix*, Fig. S4*C*).

Effect of FITC Conjugation Site and Valency on Anti-FITC CAR-T Cells in Vitro Activity. Next, we evaluated the ability of the anti-CD19 Fab switches to induce anti-FITC CAR–T-cell effector functions. Highly potent lytic activity was induced by all FITC conjugates against Nalm-6 cells (human $CD19^+$ B-acute lymphoblastic leukemia line) in a dose-dependent manner. However, differences in cytotoxicity were observed depending on conjugation sites: FITC conjugates proximal to the antigen binding region (EC_{50}; A = 0.9 ± 0.3 pM and B = 0.5 ± 0.1 pM) were more potent than switches conjugated at distal sites (EC_{50}; E = 2.9 ± 0.4 pM and F = 4.0 ± 0.2 pM) (Fig. 1*B*). This trend was consistently observed in cytotoxicity assays using different cancer cell lines (Daudi and IM-9) with varied CD19

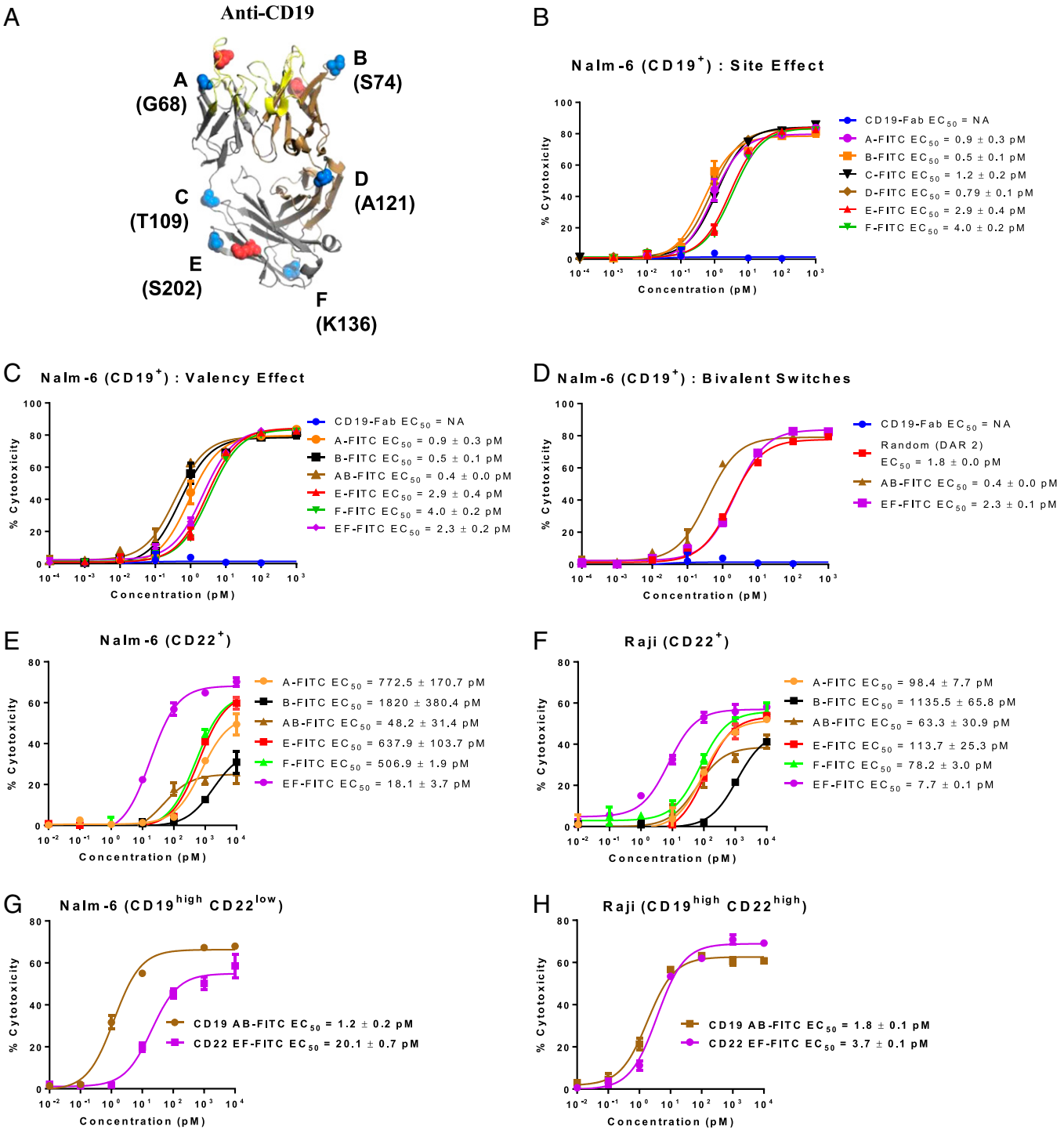

Fig. 1. Anti-CD19 and anti-CD22 antibody FITC conjugates. (*A*) Crystal structure of a mouse Fab (clone 93f3, PDB ID code 1T4K) indicating FITC conjugation sites. Silver, light chain; gold, heavy chain; yellow, variable binding region; blue, sites of pAzF incorporation allowing for site specific conjugation; red, sites modified by random NHS conjugation. (*B–D*) Anti-FITC CAR-T cells and Nalm-6 cells were cocultured at a 5:1 ratio, respectively, with different concentrations of anti-CD19 FITC conjugates in cytotoxicity assays. One representative experiment is shown to demonstrate the impact of (*B*) conjugation site, (*C*) valency, and (*D*) conjugation method (site-specific vs. random) on CAR–T-cell activity. Cytotoxicity assays comparing (*E* and *F*) conjugation sites and valency of anti-CD22 FITC conjugates against $CD22^{+}$ target cells, and (*G* and *H*) optimized CD19- and CD22-targeting switches against tumor cell lines with differential antigen expression levels: Nalm-6 ($CD19^{high}$, $CD22^{low}$) and Raji ($CD19^{high}$, $CD22^{high}$). Each data point represents a mean of duplicate samples, and error bars represent SD. Results shown are a representative of three independent experiments.

expression levels and with different CAR-T cells generated from three healthy donors (*SI Appendix*, Fig. S5 *A–C*). The bivalent switches (EC_{50}; AB = 0.4 ± 0.0 pM and EF = 2.3 ± 0.2 pM) were more potent than their corresponding monovalent FITC switches (Fig. 1*C*). The random FITC conjugate induced lytic activity (EC_{50} = 1.8 ± 0.0 pM) that was comparable to the site-specific EF switch, but significantly less than the site-specific AB switch (Fig. 1*D*). These results show that the site and stoichiometry of conjugation of

FITC to anti-CD19 Fab affect the anti-FITC CAR-T activity. Nonconjugated CD19 Fabs failed to induce lysis of Nalm-6 cells, and no significant cytotoxic activity was observed with K562 ($CD19^-$) cells for any site-specifically conjugated switch (*SI Appendix*, Fig. S5*A*). In addition to lytic function, all FITC conjugates induced IFN-γ, TNF, and IL-2 release that correlated with the degree of cytotoxicity, with the AB-FITC switch yielding the highest cytokine induction (*SI Appendix*, Fig. S5*D*). Finally, to confirm the specificity of the AB-FITC switch, we performed competition assays using excess anti-CD19 (IgG, clone FMC63) antibody or free FITC (*SI Appendix*, Fig. S5 *E* and *F*). With a 1,000-fold excess of anti-CD19 antibody, lytic activity of anti-FITC CAR-T cells induced with 10 pM of anti-CD19 AB-FITC was significantly reduced (from 54.0 ± 0.1% to 9.8 ± 1.1%), whereas minimal changes were observed with an isotype control antibody. Similarly, excess FITC (10 μM) also decreased CAR–T-cell cytotoxicity from 57.4 ± 3.7% to 29.5 ± 3.0% in the presence of anti-CD19 AB-FITC (10 pM). Overall, these results demonstrate that the ability to control the site and stoichiometry of FITC conjugation to the switch molecule significantly impacts CAR-T activity, with bivalent anti-CD19 AB-FITC switch inducing the most potent and selective in vitro cytotoxicity of anti-FITC CAR-T cells.

Optimization of the Anti-CD22 Switch. We next determined the feasibility of targeting other tumor antigens using the same anti-FITC CAR-T cells. CD22 is another well-characterized B-cell–associated tumor marker, which is found on most B-cell leukemias and lymphomas. To generate anti-CD22 switches, sequences of the variable region were obtained from the anti-CD22 antibody, clone M971, which has been previously incorporated into a CAR construct that showed in vivo efficacy in mouse xenograft models (38, 39). We selected proximal and distal positions similar to our CD19 switches to generate four monovalent (A, B, E, and F), as well as two bivalent (AB and EF) FITC-conjugated switches using the same semisynthetic approach described above. Interestingly, when we compared the anti–CD22-FITC switches with our anti-FITC CAR-T cells in cytotoxicity assays using Nalm-6 cells, we found that FITC conjugated to distal positions (EC_{50}; E = 0.6 ± 0.1 nM and F = 0.5 ± 0.0 nM) were more cytotoxic to $CD22^+$ cells in comparison with proximal FITC conjugates (EC_{50}; A = 0.8 ± 0.2 nM and B = 1.8 ± 0.4 nM) (Fig. 1*E*). Interestingly, these results are opposite to our previous findings with CD19 switches (Fig. 1*C*). However, as was the case with CD19, an enhancement in cytotoxicity was observed with bivalent switches (EC_{50}; EF = 18 ± 4 pM and AB = 48 ± 31 pM), but the improvement was more profound. A similar trend was observed in the cytotoxicity assays using $CD22^+$ B-cell lymphoma cells, Raji (Fig. 1*F*). This difference in CAR-T activity with different conjugation sites suggests that distinct geometries are required for each antigen–antibody interaction to realize optimal effector function. We also observed that the anti-CD19 AB-FITC switch (EC_{50}; AB = 1.2 ± 0.2 pM) is ∼20 times more efficacious on Nalm-6 than the optimized anti-CD22 EF-FITC switch (EC_{50}; EF = 20 ± 1.0 pM) (Fig. 1*G*). This result is likely because of lower CD22 expression levels on Nalm-6 cells, as previously reported (*SI Appendix*, Fig. S5*G*) (39). Indeed, when we compared both optimized switches in cytotoxicity assays using $CD22^{high}$-expressing Raji cells, similar cytotoxicity was observed (EC_{50} = 1.8 ± 0.1 pM and 3.7 ± 0.1 pM, respectively) (Fig. 1*H*). Taken together, these results demonstrate that homogeneous, site-specific FITC-based switches can be readily optimized using a single CAR-T cell to enable highly effective geometries for CAR-T and tumor cell interactions, regardless of antigen–antibody pairing.

CART-19 vs. sCAR-T Cells: In Vitro and in Vivo Comparison. To determine the relative activity of our sCAR-T cells with a conventional CAR, we compared cytotoxicity and activation markers with a second-generation CD19-specific CAR currently in clinical trials, which uses the same FMC63 anti-CD19 scFv (CART-19) (*SI Appendix*, Fig. S6*A*) (1, 30, 31). Anti-FITC and anti-CD19 CAR lentiviral particles were generated and used to transduce T cells from the same donor (∼50–60% transduction efficiency, 7 d post-transduction). To minimize the effect of differential CAR expression, both CAR-T cells were affinity-purified (>90% purity) (*SI Appendix*, Fig. S6*B*) and used for in vitro and in vivo efficacy studies. With 1 nM anti-CD19 AB-FITC, anti-FITC CAR-T cells lysed Nalm-6 cells to a similar extent as CART-19 in 24-h cytotoxicity assays at varying effector to target (E:T) cell ratios (Fig. 2*A*). Similarly, as shown in *SI Appendix*, Fig. S6*E* and Fig. 2*B*, we observed comparable up-regulation of activation markers (CD69 and CD25) and release of cytokines. We also assessed the induction of the anti-apoptotic marker Bcl-xL, which is a hallmark of 4-1BB costimulatory signaling (40). As shown in *SI Appendix*, Fig. S6*F*, an induction of Bcl-xL is observed in both CAR-T cells. Moreover, in all experiments, activity of both CAR-T cells was observed only in the presence of $CD19^+$ tumor cells (*SI Appendix*, Fig. S6 *C–F*). Overall, our in vitro findings suggest that anti-FITC CAR-T cells, in conjunction with the optimized anti-CD19 AB-FITC switch, are comparable to conventional CD19 targeting CAR-T cells (CART-19) in eliciting tumor-specific effector functions as well as inducing costimulatory signaling.

We next tested our CD19-targeting CAR-T cells in a Nalm-6 xenograft model. Briefly, 0.5×10^6 Nalm-6 cells transduced with luciferase were injected intravenously into female NOD.Cg-*Prkdc*^{scid} *Il2rg*^{tm1Wjl}/SzJ mice (NSG). Seven days later, mice were infused with 40×10^6 CAR-T cells intravenously and switch treatment was initiated with indicated anti-CD19 FITC conjugates at 0.5 mg/kg (intravenously) or PBS (intravenously) every other day for a total of six doses (Fig. 2*C*). Tumor growth was monitored weekly by bioluminescence imaging. After three doses of anti-CD19 AB-FITC, mice infused with anti-FITC CAR-T cells cleared tumor to the same extent as CART-19, and both groups of mice remained tumor-free for greater than 60 d (Fig. 2*D*). In addition to the proximal bivalent anti-CD19 AB-FITC, we also evaluated selected monovalent (B and E) and bivalent (EF and random DAR 2) switches. As shown in Fig. 2 *C* and *D*, the in vivo activity of the switches correlated with our previous in vitro data but the differences were more pronounced: the anti-CD19 B-FITC initially exhibited antitumor efficacy; however, tumor relapse was observed on day 47 of the study; random and distal conjugates (E- and EF-FITC) delayed tumor growth but did not clear tumors. It is noteworthy that the B switch substantially outperformed bivalent EF and random switches, reaffirming the importance of the conjugation site on efficacy. Rapid tumor growth was observed in mice treated with PBS or nonconjugated anti-CD19 antibody, which confirms that the antitumor response is FITC switch-dependent. Importantly, this study demonstrates that our sCAR-T cells can achieve excellent in vivo antitumor activity.

Control of in Vivo sCAR-T Activity. We next determined whether the in vivo activity of our sCAR-T cells can be regulated in a switch dose-dependent manner. Briefly, mice with established Nalm-6 tumor burden received anti-FITC CAR-T cells (40×10^6) as described above, and anti-CD19 AB-FITC switches were injected at doses ranging from 0.005 to 0.5 mg/kg every other day over 12 d (day 7 to day 17). Consistent with the previous study, mice treated with the effective dose (0.5 mg/kg) achieved rapid tumor clearance (Fig. 3*A* and *SI Appendix*, Fig. S7*A*). A reduction in tumor burden was initially observed with animals that received 0.05-mg/kg switch; however, this group relapsed after treatment with six doses and succumbed to disease at day 48. When we extended the 0.05-mg/kg treatment up to 12 doses, tumor growth was stabilized but complete tumor clearance was not observed (*SI Appendix*, Fig. S8). Further decrease in switch dose (0.005 mg/kg) had minimal effect in this disease model. The expansion of anti-FITC CAR-T cells correlated with the observed dose-dependent antitumor activity (Fig. 3*B*): after receiving six doses (day 18), animals treated with the highest dose (0.5 mg/kg) had an

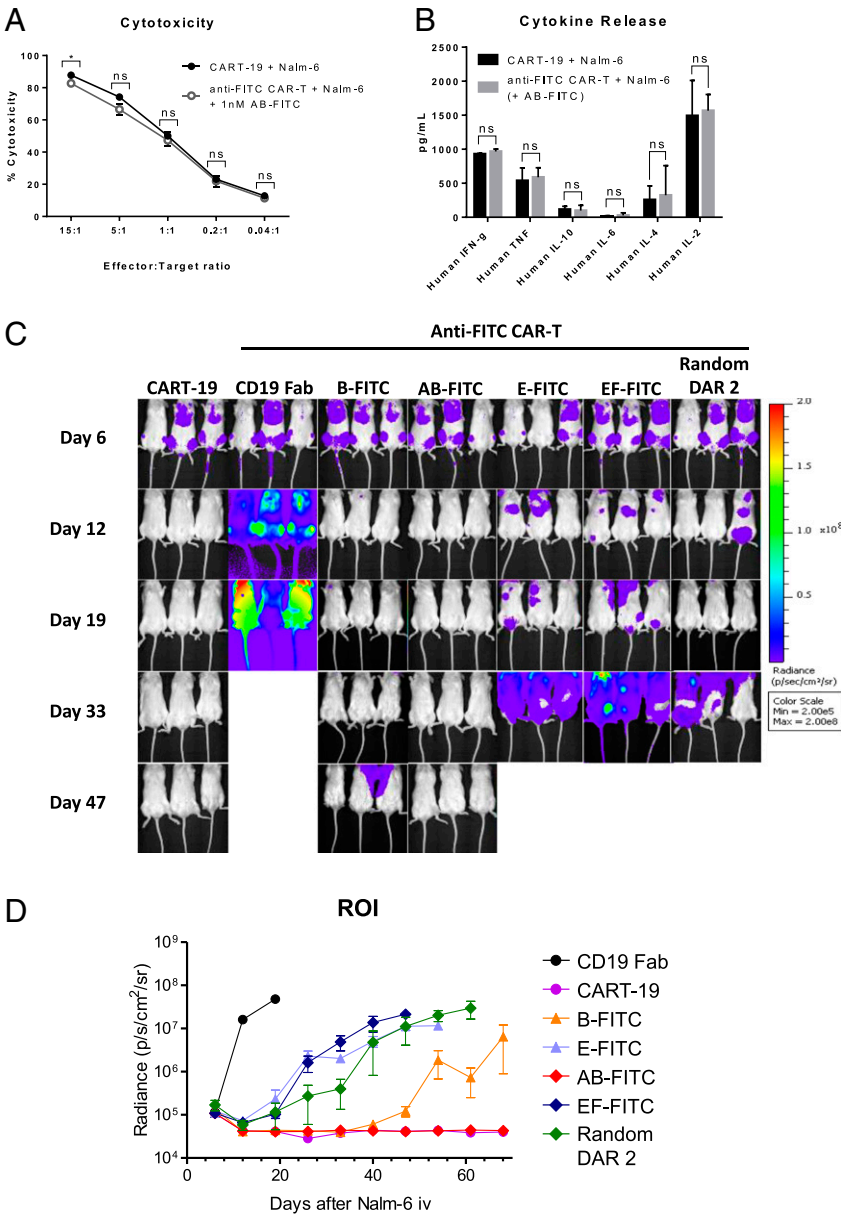

Fig. 2. In vitro and in vivo comparison of CART-19 and anti-FITC CAR-T cells with optimized anti-CD19 AB-FITC switch. (*A*) Anti-FITC CAR-T cells and Nalm-6 ($CD19^+$) cells were cocultured for 24 h at indicated E:T ratios with 1 nM of anti-CD19 AB-FITC switch, and target cell lysis was determined by flow cytometry, as described in *SI Appendix, SI Methods*. (*B*) Indicated cytokines were measured in supernatant from activation assays (*SI Appendix*, Fig. S6*E*) using BD Cytometric Bead Array (CBA) Human Th1/Th2 II Kit according to manufacturer's protocol. All results are representative of independent experiments with CAR-T cells generated from three different donors. Data shown are an average of duplicate or triplicate samples, and error bars represent SD. ns = $P > 0.05$ and $^*P < 0.05$ were calculated using one-tailed Student's *t* test. (*C* and *D*) 0.5×10^6 Nalm-6 cells transfected with luciferase were injected intravenously into 6- to 8-wk-old female NSG mice. Seven days later, mice were infused with 40×10^6 CAR-T cells intravenously and switch treatment was initiated with indicated anti-CD19 FITC conjugates at 0.5 mg/kg or PBS every other day for a total of six doses (intravenously). (*C*) Tumor burden was monitored by weekly bioluminescence imaging (BLI), and (*D*) quantified by the radiance detected in the region of interest (ROI). Results are derived from six mice per group, and error bars represent SD.

~sevenfold increase in $CD3^+$ cells compared with mice that received the lowest dose (0.005 mg/kg). The expansion of human T cells was tumor-dependent, as demonstrated by the ~fourfold higher T-cell number observed in tumor-bearing mice in comparison with disease-free mice. These results indicate that the in vivo sCAR–T-cell activity and expansion can be controlled by switch dose. In these dose-titration studies, mice that received CART-19 or anti-FITC CAR-T cells with the anti-CD19 AB-FITC switch at 0.5 mg/kg dose exhibited significant body weight loss (≥10%) shortly after the initiation of treatment (*SI Appendix*, Fig. S7*B*), which resolved within 4 d (*SI Appendix*, Fig. S7*C*). Conversely, mice treated with suboptimal switch doses (0.05 and 0.005 mg/kg) did not display similar signs of distress. This acute toxicity is likely related to the antitumor activity elicited by CAR-T cells, because our control group, healthy mice injected with anti-FITC CAR-T cells and 0.5 mg/kg of anti-CD19 AB-FITC, did not exhibit any signs of toxicity (*SI Appendix*, Fig. S7 *B* and *C*).

Adverse events such as severe CRS have been associated with the administration of CAR-T cells to patients with high tumor burden, which likely triggers massive antigen-specific CAR–T-cell expansion and activation (4, 41). Therefore, we next asked whether the switch could be dose-titrated to achieve a gradual tumor

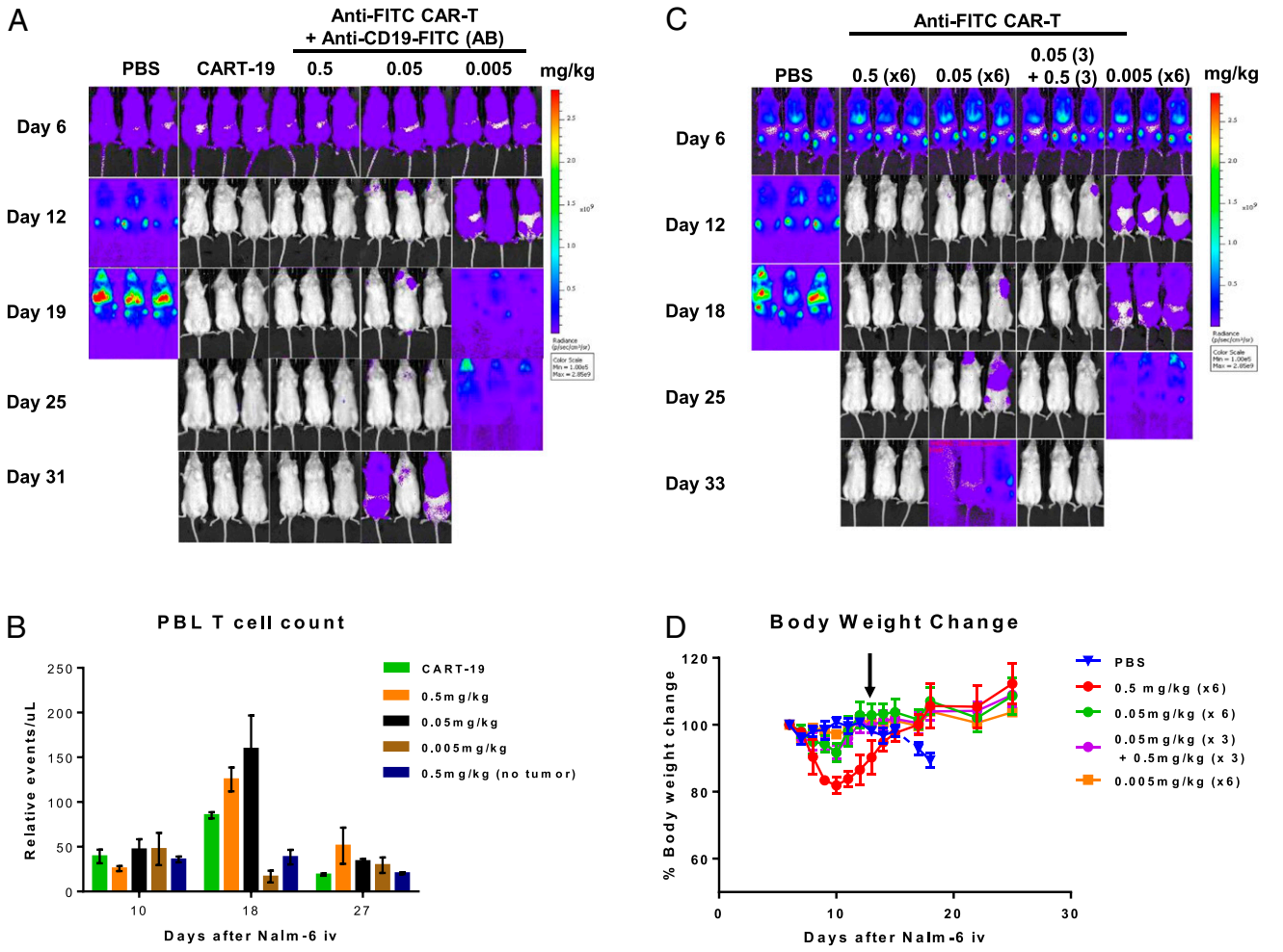

Fig. 3. Dose titratable in vivo response of anti-FITC CAR-T cells achieved with anti-CD19 AB-FITC switch. (*A*) BLI of NSG mice inoculated with 0.5×10^6 Nalm-6 cells on day 1, and infused with 40×10^6 CART-19 or anti-FITC CAR-T cells on day 7. On the same day, switch treatment was initiated at indicated doses at every other day for six doses. Tumor-bearing mice treated with vehicle (PBS) were included as a negative control. (*B*) $CD3^+$ peripheral blood lymphocyte (PBL) count from weekly retro-orbital bleeds after treatment with anti-CD19 AB-FITC as described in *SI Appendix, SI Methods*. As a control for potential nonspecific T-cell expansion, disease-free mice were injected with anti-FITC CAR-T cells and received six doses of anti–CD19-FITC (0.5 mg/kg). Averages and error bars represent SD derived from three to four mice from each group. (*C*) BLI of NSG mice inoculated with Nalm-6 cells, and infused anti-FITC CAR-T cells as described in *A*. On day 7, anti-CD19 AB-FITC treatment was initiated at indicated doses and continued every other day. Parentheses indicate the total number of doses that each group received. Arrow specifies time of increase in switch dose from 0.05 to 0.5 mg/kg. (*D*) Percentage of body weight change observed from *C*. Data points and error bars represent average and SD derived from six mice per group, respectively.

clearance to avoid the acute toxicity. In these dose-escalation studies, treatment of tumor-bearing mice was initiated with the effective (0.5 mg/kg) or suboptimal (0.05 mg/kg) dose (Fig. 3*C*). In agreement with our previous findings, significant body weight loss was observed in mice treated with a starting dose at 0.5 mg/kg of anti-CD19 AB-FITC, whereas mice treated with 0.05 mg/kg did not lose weight to a similar extent (Fig. 3*D*). Furthermore, evaluation of serum cytokines ∼24 h after CAR-T cells and switch injections revealed a dose-dependent elevation of human (IFN-γ, TNF, and IL-2) and mouse (MCP-1) cytokines (*SI Appendix*, Fig. S9*B*). After three doses, animals that received 0.05 mg/kg of AB-FITC were further divided into two groups: (*i*), in which the switch dose was maintained at 0.05 mg/kg, or (*ii*), in which treatment was continued with an elevated switch dose (0.5 mg/kg). Given that a majority of the tumor burden was reduced with the first three suboptimal doses of 0.05 mg/kg, the subsequent increase in switch dose to 0.5 mg/kg did not result in significant weight loss (Fig. 3*D* and *SI Appendix*, Fig. S9*A*). More importantly, our dose-escalation regimen achieved tumor clearance comparable to animals that were started with high dose switch (0.5 mg/kg) (Fig. 3*C* and *SI Appendix*, Fig. S9*A*). Collectively, our results demonstrate that the activity of sCAR-T cells can be controlled by switch dosage to minimize treatment-related toxicities while retaining potent anti-tumor activity. This ability to control the temporal activation of the CAR–T-cell response may be helpful clinically to ameliorate adverse events associated with the administration of CAR-T cells to patients with high tumor burden, such as severe CRS (4, 41).

Overcoming B-Cell Aplasia by Termination of Switch Dosing. In addition to CRS, another major safety issue associated with current CART-19 therapy is the persistent ablation of normal B cells. Therefore, we asked whether the CAR-T switch platform could be used to minimize this "on-target"-related adverse event. Toward this end, we generated a second-generation mouse surrogate anti-FITC CAR based on the reported anti-mouse CD19 CAR vector, which encodes for anti-mouse CD19 scFv (clone 1D3) and mouse signaling domains (CD28 and CD3ζ) in a retroviral backbone (*SI Appendix*, Fig. S10*A*). Murine anti-FITC CAR-T cells were generated using splenocytes from immunocompetent C57BL/6 mice, as previously described (42), and tested for cytotoxicity against

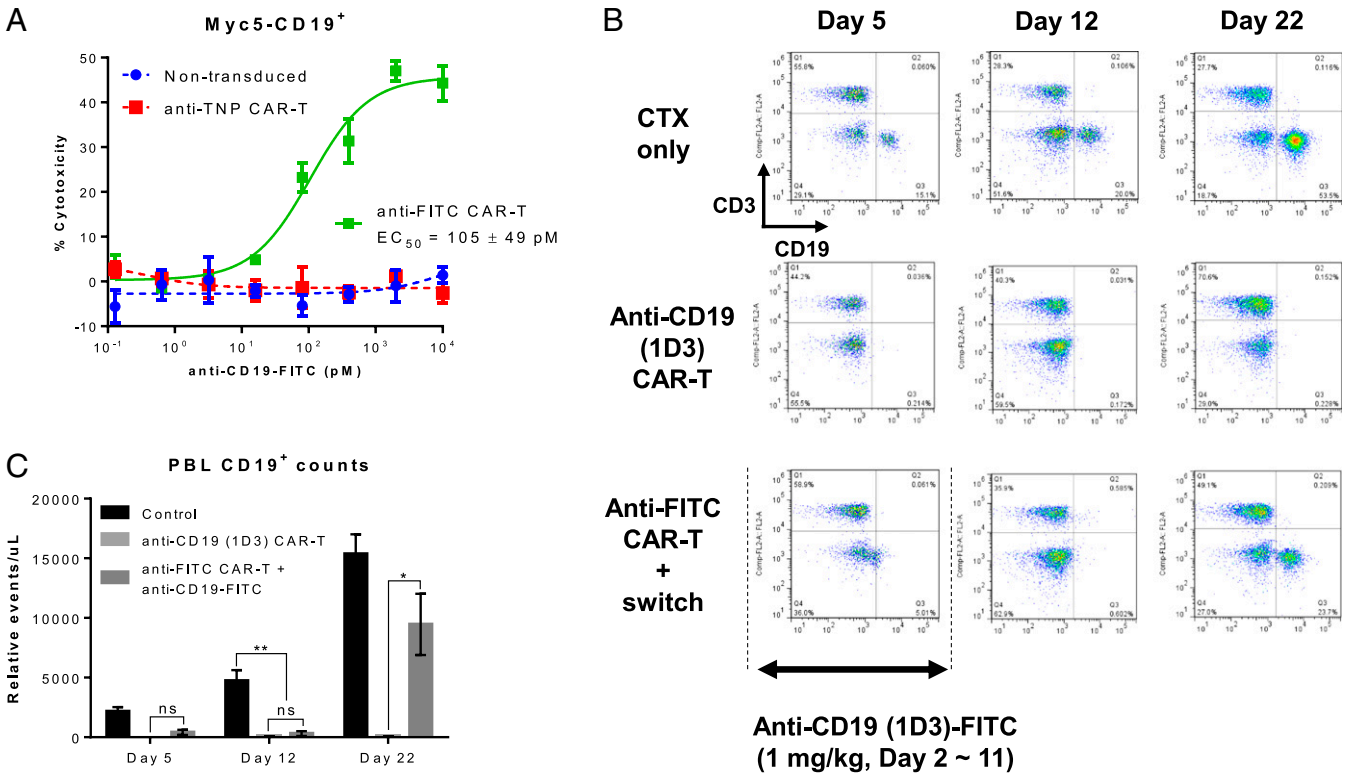

Fig. 4. In vivo efficacy and safety of mouse anti-FITC CAR-T cells with anti-mouse CD19 (1D3)-FITC switch. (*A*) Cytotoxicity assay using mouse anti-FITC CAR-T cells and Myc5 $CD19^+$ cells cocultured at a 10:1 ratio, respectively, in the presence of different concentrations of indicated anti-CD19 (1D3)-FITC switch. Nontransduced mouse T cells and mouse T cells transduced with an irrelevant anti-TNP CAR served as negative controls. Each data point represents a mean of triplicate samples, and error bars represent SEM. Results presented are representative of three independent experiments. (*B* and *C*) Flow cytometry analysis of $CD3^+$ or $CD19^+$ cells in mice treated with anti-CD19 (1D3) CAR-T or anti-FITC CAR-T with anti-CD19 (1D3)-FITC switch. C57BL/6 mice were preconditioned with cyclophosphamide (150 mg/kg) on day 1, and received 6×10^6 syngeneic anti-CD19 (ID3) CAR or anti-FITC CAR-T cells by tail-vein injections the next day. Daily treatments with anti-mouse CD19 (1D3)-FITC switch at 1 mg/kg were initiated the same day as CAR–T-cell infusions for a total of 10 injections (days 2–11). Weekly retro-orbital bleeds were carried out to assess $CD3^+$ and $CD19^+$ cells. (*B*) Dot plots are a representative of five to six mice per group. (*C*) Graphical representation of $CD19^+$ cells quantified from *B*. Results are displayed as an average of five to six mice, and error bars represent SD. ns = $P > 0.05$, $^*P < 0.05$, and $^{***}P < 0.0005$ were calculated using one-tailed Student's *t* test.

$CD19^+$ Myc5 cells in the presence of an anti-mouse CD19 (1D3) FITC switch conjugated at the distal position of the light chain (Ser202). As shown in Fig. 4*A*, mouse anti-FITC CAR-T cells induced switch-dependent target cell lysis (EC_{50} = 105 ± 49 pM). No activity was observed with nontransduced mouse T cells or with a CAR-T cell specific for 2,4,6-trinitrophenyl (TNP) group in the presence of murine anti-CD19 switch.

We next established the activity of this CAR-T in a surrogate B-cell depletion model. In this model, C57BL/6 mice were preconditioned with cyclophosphamide (150 mg/kg) on day 1. The next day, 6×10^6 of syngeneic anti-mouse CD19 or anti-FITC CAR-T cells (~75% transduction efficiency) were infused. Mice that had received anti-FITC CAR-T cells were injected daily intravenously with anti-mouse CD19 FITC switch at 1 mg/kg (days 2–11). To assess the depletion of B cells, $CD3^+$ and $CD19^+$ cells in peripheral blood were monitored by flow cytometry (Fig. 4 *B* and *C*). By day 5 of the study (after three injections of switch), peripheral B-cell loss was observed in both CAR-T groups. On day 12 of the study, switch treatment was halted and animals were monitored for repopulation of $CD19^+$ cells. In agreement with previous reports (42, 43), we observed a persistent loss of $CD19^+$ cells with the anti-mouse CD19 CAR (up to day 22). By contrast, there was repopulation of $CD19^+$ cells in the peripheral blood of animals treated with the anti-FITC CAR-T in adjunct with anti-CD19 FITC switch on day 22 (11 d after the last dose of switch) (Fig. 4 *B* and *C*). This study demonstrates that a sCAR-T approach allows the CAR-T response to be "turned-off" by discontinuation of switch dosing once the desired efficacy is achieved, and can potentially prevent adverse effects associated with the persistent activity of CAR-T cells.

Discussion

CAR–T-cell therapy has emerged as a promising experimental therapy for patients with B-cell malignancies. However, the inability to control the activity of CAR-T cells in vivo has resulted in treatment-related toxicities. To address this limitation, the use of soluble intermediate "switch" molecules (e.g., hapten-labeled or unmodified therapeutic monoclonal antibodies) has been explored by several groups to regulate CAR-T cells (17–19). Although these studies have demonstrated the feasibility of redirecting CAR–T-cell activity with switch molecules, the methods used to generate these switches do not in general allow for facile modulation of CAR-T activity. Moreover, the dose-titratable control of sCAR–T-cell in vivo activity, which may be important for addressing safety issues related to CAR-T therapy, has not been evaluated in these studies.

Herein, we report a general approach to optimize hapten-based sCAR-Ts. Using a site-specific protein-conjugation method, we generated a panel of homogeneously FITC-labeled antibody switches that mediate distinct spatial interactions between sCAR-T and cancer cells (12, 21, 22, 39, 44, 45). We first applied this approach to optimize a switch to target the B-cell surface antigen, CD19, a well-studied and validated antigen for conventional CAR-T therapies. In our in vitro studies, site-specifically conjugated

anti-CD19 FITC switches derived from the anti-CD19 clone FMC63 were found to induce CD19-targeted CAR–T-cell activity to varying degrees depending upon the site of FITC conjugation to the antibody molecule. In particular, when FITC molecules were conjugated to sites on the Fab proximal (A and B) to the antigen-binding domain, the resulting switches induced greater antitumor activity in comparison with intermediate (C and D) or distal (E and F) sites, relative to the antigen-binding domain. Although the structure of CD19 and epitope bound by the antibody FMC63 are unknown, this finding suggests that proximal conjugation sites likely lead to a shorter distance between anti-FITC CAR-T cells and $CD19^+$ cells that results in enhanced antitumor activity. Notably, previous studies with anti-CD3 bispecific antibodies have also reported that close proximity between T cells and the target cell membrane significantly enhances the efficacy of these antibodies (46). More importantly, our in vitro observations regarding site specificity for optimal target cell killing were confirmed in vivo. The bivalent anti-CD19 AB-FITC switch in which the FITC conjugation was near the antigen-binding domain was the most efficacious form when combined with anti-FITC CAR-T cells and achieved a potent antitumor response in our Nalm-6 xenograft model.

In addition to CD19, we also generated switches targeting another well-established B-cell antigen, CD22, to determine the general applicability of our optimization process. In contrast to our findings with the anti-CD19 switch, we found that distal conjugation sites (E and F) afforded the most potent in vitro antitumor activity when targeting CD22 with the Fab switches derived from the M971 antibody. A potential reason for this difference could be inferred from the epitope of the M971 antibody, which is located at the membrane proximal region of CD22 (47). Thus, access of the anti-FITC scFv to A and B sites on M971 Fab could be sterically hindered by the large extracellular domain (~75 kDa) of CD22, whereas the distal conjugation sites (E and F) likely provide the necessary geometry to enable optimal target and CAR-T cell interaction. Overall, the results from anti-CD19 and anti-CD22 switch optimization suggest that the difference in optimal conjugation sites is likely a reflection of the need to create a pseudo-immunological synapse that is similar in distance to physiological T-cell receptor/MHC complexes, which is reportedly ~130–150 Å (48), while maintaining accessibility to anti-FITC scFv.

One commonality observed with both anti-CD19 and anti-CD22 switches is that bivalent (AB and EF, respectively) switches consistently outperform the corresponding monovalent switches, which may be attributable to the higher affinity for anti-FITC scFv or the potential to induce in situ dimerization of CAR. Indeed, in our accompanying studies using peptide neo-epitope grafted switches, antipeptide neo-epitope CAR–T-cell activity was improved when a mutation was introduced within the hinge region to enhance the dimerization of CAR via interchain disulfide bond (44, 49). Notably, despite a similar FITC to antibody ratio (average DAR ~2), the randomly conjugated anti-CD19 FITC switch demonstrated inferior in vivo antitumor activity relative to the optimized bivalent anti-CD19 AB-FITC switch, highlighting the importance of a site-specific conjugation approach to generate optimized switches.

To establish whether the in vivo sCAR–T-cell activity can be controlled with a switch, we evaluated our approach in Nalm-6 tumor xenograft models. In these studies, switch-mediated antitumor activity and proliferation of CAR-T cell was strictly switch dose-dependent. More importantly, we demonstrated that treatment-related toxicities, such as body weight loss and elevated serum cytokines, were also switch-dose related. Although the observed toxicities resembled CRS reported in patients that had received CD19-targeting T-cell–based therapies, we found differences in serum cytokine profiles, for example IL-6, which is typically elevated in human CRS, was not detectable in our model. In addition, elevated levels of uric acid and phosphate, indicators of tumor lysis syndrome, were not found. However, these different manifestations of CAR-related toxicities may be a reflection of the missing immune components in immunocompromised NSG mice (41). Nonetheless, our preclinical studies demonstrate that controlling in vivo CAR-T activity via a switch dosing regimen may improve the safety profile while preserving the potent antitumor response.

Overcoming toxicities related to persistent CAR–T-cell activity, such as B-cell aplasia, was also demonstrated with our sCART approach. In immunocompetent mice, we showed that CD19-targeting by CAR-T cells is reversible by simply terminating switch dosing. Furthermore, our demonstration of the reversibility of CAR–T-cell activity in surrogate models may expand the potential application of the sCAR-T approach to other indications, such as acute myeloid leukemia and solid tumors, to which the long-term persistence of CAR-T cells may pose a greater safety risk (50).

In conclusion, we have demonstrated a general method for producing site-specifically conjugated antibody-FITC switches that elicit potent anti-FITC CAR–T-cell effector functions. Furthermore, we showed that the ability to chemically define specific conjugation sites significantly influenced the efficacy of anti-CD19 and anti-CD22 switch molecules. We also showed the versatility of our platform by targeting two different antigens with a single CAR. This aspect of our strategy should be useful in treating tumor escape variants (1) or heterogeneous tumors expressing distinct tumor antigens, and also can simplify manufacturing of CAR-Ts for different indications (single CAR-encoding vector). Importantly, using an optimized sCAR-T system for CD19, we achieved potent in vivo antitumor activity in a xenograft model. In addition, we demonstrated that our switchable approach may provide a way to prevent or manage major safety issues associated with current CD19 targeting CAR therapies, such as severe CRS and long-term B-cell depletion. Finally, the ability to regulate in vivo activity as well as the specificity of engineered T cells with a soluble intermediate switch may allow for the safe application of this potent immune cell-based therapy to target other types of cancer, including solid tumors, as well as nononcology indications.

Methods

Xenograft Studies. All procedures described herein were approved by the California Institute for Biomedical Research Institutional Animal Care and Use Committee and were performed according to national and institutional guidelines for the humane treatment of animals. Six- to 8-wk-old female NOD.Cg-*Prkdc*^{scid} *Il2rg*^{tm1Wjl}/SzJ (NSG) mice were intravenously inoculated with 0.5×10^6 Nalm-6 cells transfected with luciferase (kindly provided by J.N.K., National Cancer Institute, Bethesda) and engraftment was confirmed by bioluminescence imaging. The next day, CAR-T cells were infused and treatment with indicated anti-CD19 (clone FMC63) FITC switches was initiated. In parallel, control groups (tumor only, CAR-T cells only, and tumor-bearing mice that received CART-19 T cells) were injected with PBS. Body weight was monitored daily, and tumor growth was monitored weekly by bioluminescence imaging.

The expansion of human T cells in the peripheral blood was monitored using weekly retro-orbital bleeds. Briefly, 40 μL of blood was incubated with PE-conjugated anti-CD3 (OKT3) conjugated at room temperature for 30 min. Next, red blood cells were lysed with 10× FACS Lysing Solution (BD Biosciences) according to the manufacturer's instructions and remaining lymphocytes were washed with staining buffer. Liquid counting beads (BD Biosciences) were added before analysis on a BD Accuri C6, where 33 μL of 330 μL was acquired from each sample. To enumerate the number of $CD3^+$ cells per microliter of blood, we used the following formula: relative $CD3^+$ events per microliter = [no. of $CD3^+$ events × percentage of acquired volume]/[volume of blood used for staining (μL)].

To determine whether the initial weight loss observed is associated with an elevated systemic cytokines or increased tumor lysis, serum from retro-orbital bleeds taken 24 h after the initial switch treatment were used. Serum cytokines were quantified using BD CBA Human Th1/Th2 Kit II and Mouse Inflammation Kit according to product manuals. Uric acid and phosphate levels were also assessed using fluorescent-based assay kits (Abcam), but inconclusive results were obtained.

Surrogate Studies. To facilitate the engraftment of CAR-T cells, 6- to 8-wk-old C57BL/6 mice were preconditioned with 150 mg/kg of cyclophosphamide (Sigma) on day 1. The next day, 6×10^6 syngeneic anti-FITC CAR-T cells and anti-CD19 (1D3) FITC switch (1 mg/kg) were sequentially administered by tail-vein injections. Thereafter, switch molecules were injected daily at 1 mg/kg for a total of 10 doses (days 2–11). As a positive control, a separate cohort of mice received T cells transduced with the conventional anti-mouse CD19 (ID3) CAR. To assess the efficacy and specificity of mouse sCAR-T cells, $CD3^+$ and $CD19^+$ populations in the peripheral blood were monitored once a week for the duration of the study using PE-conjugated anti-mouse CD3 (2C11, Biolegend) and FITC-conjugated anti-mouse CD19 (6D5, Biolegend), to evaluate the loss and repopulation of B cells during and after treatment, respectively. Unstained and single color controls were acquired and used for compensation.

ACKNOWLEDGMENTS. We thank Dr. Andrei Thomas-Tikhonenko (University of Pennsylvania) for providing murine CD19-overexpressing Myc5 cells, and Dr. Inder Verma for his assistance with lentiviral constructs.

1. Grupp SA, et al. (2013) Chimeric antigen receptor-modified T cells for acute lymphoid leukemia. *N Engl J Med* 368(16):1509–1518.
2. Davila ML, et al. (2014) Efficacy and toxicity management of 19-28z CAR T cell therapy in B cell acute lymphoblastic leukemia. *Sci Transl Med* 6(224):224ra25.
3. Barrett DM, Singh N, Porter DL, Grupp SA, June CH (2014) Chimeric antigen receptor therapy for cancer. *Annu Rev Med* 65:333–347.
4. Maude SL, Barrett D, Teachey DT, Grupp SA (2014) Managing cytokine release syndrome associated with novel T cell-engaging therapies. *Cancer J* 20(2):119–122.
5. Tey SK (2014) Adoptive T-cell therapy: Adverse events and safety switches. *Clin Transl Immunology* 3(6):e17.
6. Kochenderfer JN, et al. (2012) B-cell depletion and remissions of malignancy along with cytokine-associated toxicity in a clinical trial of anti-CD19 chimeric-antigen-receptor-transduced T cells. *Blood* 119(12):2709–2720.
7. Kochenderfer JN, et al. (2010) Eradication of B-lineage cells and regression of lymphoma in a patient treated with autologous T cells genetically engineered to recognize CD19. *Blood* 116(20):4099–4102.
8. Morgan RA, et al. (2010) Case report of a serious adverse event following the administration of T cells transduced with a chimeric antigen receptor recognizing ERBB2. *Mol Ther* 18(4):843–851.
9. Lamers CH, et al. (2013) Treatment of metastatic renal cell carcinoma with CAIX CAR-engineered T cells: Clinical evaluation and management of on-target toxicity. *Mol Ther* 21(4):904–912.
10. Parkhurst MR, et al. (2011) T cells targeting carcinoembryonic antigen can mediate regression of metastatic colorectal cancer but induce severe transient colitis. *Mol Ther* 19(3):620–626.
11. Morgan RA, et al. (2013) Cancer regression and neurological toxicity following anti-MAGE-A3 TCR gene therapy. *J Immunother* 36(2):133–151.
12. Kenderian SS, et al. (2015) CD33-specific chimeric antigen receptor T cells exhibit potent preclinical activity against human acute myeloid leukemia. *Leukemia* 29(8): 1637–1647.
13. Di Stasi A, et al. (2011) Inducible apoptosis as a safety switch for adoptive cell therapy. *N Engl J Med* 365(18):1673–1683.
14. Wilkie S, et al. (2012) Dual targeting of ErbB2 and MUC1 in breast cancer using chimeric antigen receptors engineered to provide complementary signaling. *J Clin Immunol* 32(5):1059–1070.
15. Fedorov VD, Themeli M, Sadelain M (2013) PD-1- and CTLA-4-based inhibitory chimeric antigen receptors (iCARs) divert off-target immunotherapy responses. *Sci Transl Med* 5(215):215ra172.
16. Wu CY, Roybal KT, Puchner EM, Onuffer J, Lim WA (2015) Remote control of therapeutic T cells through a small molecule-gated chimeric receptor. *Science* 350(6258): aab4077.
17. Kudo K, et al. (2014) T lymphocytes expressing a CD16 signaling receptor exert antibody-dependent cancer cell killing. *Cancer Res* 74(1):93–103.
18. Tamada K, et al. (2012) Redirecting gene-modified T cells toward various cancer types using tagged antibodies. *Clin Cancer Res* 18(23):6436–6445.
19. Urbanska K, et al. (2012) A universal strategy for adoptive immunotherapy of cancer through use of a novel T-cell antigen receptor. *Cancer Res* 72(7):1844–1852.
20. Kim MS, et al. (2015) Redirection of genetically engineered CAR-T cells using bifunctional small molecules. *J Am Chem Soc* 137(8):2832–2835.
21. Hudecek M, et al. (2013) Receptor affinity and extracellular domain modifications affect tumor recognition by ROR1-specific chimeric antigen receptor T cells. *Clin Cancer Res* 19(12):3153–3164.
22. Guest RD, et al. (2005) The role of extracellular spacer regions in the optimal design of chimeric immune receptors: evaluation of four different scFvs and antigens. *J Immunother* 28(3):203–211.
23. van Dam GM, et al. (2011) Intraoperative tumor-specific fluorescence imaging in ovarian cancer by folate receptor-α targeting: First in-human results. *Nat Med* 17(10): 1315–1319.
24. Herron JN, et al. (1994) High resolution structures of the 4-4-20 Fab-fluorescein complex in two solvent systems: Effects of solvent on structure and antigen-binding affinity. *Biophys J* 67(6):2167–2183.
25. Jung S, Plückthun A (1997) Improving in vivo folding and stability of a single-chain Fv antibody fragment by loop grafting. *Protein Eng* 10(8):959–966.
26. Boder ET, Midelfort KS, Wittrup KD (2000) Directed evolution of antibody fragments with monovalent femtomolar antigen-binding affinity. *Proc Natl Acad Sci USA* 97(20): 10701–10705.
27. Vaughan TJ, et al. (1996) Human antibodies with sub-nanomolar affinities isolated from a large non-immunized phage display library. *Nat Biotechnol* 14(3):309–314.
28. Maus MV, et al. (2013) T cells expressing chimeric antigen receptors can cause anaphylaxis in humans. *Cancer Immunol Res* 1(1):26–31.
29. Kalos M, et al. (2011) T cells with chimeric antigen receptors have potent antitumor effects and can establish memory in patients with advanced leukemia. *Sci Transl Med* 3(95):95ra73.
30. Maude SL, et al. (2014) Chimeric antigen receptor T cells for sustained remissions in leukemia. *N Engl J Med* 371(16):1507–1517.
31. Porter DL, Levine BL, Kalos M, Bagg A, June CH (2011) Chimeric antigen receptor-modified T cells in chronic lymphoid leukemia. *N Engl J Med* 365(8):725–733.
32. Spiegelberg HL, Weigle WO (1965) The catabolism of homologous and heterologous 7s gamma globulin fragments. *J Exp Med* 121:323–338.
33. Kim CH, Axup JY, Schultz PG (2013) Protein conjugation with genetically encoded unnatural amino acids. *Curr Opin Chem Biol* 17(3):412–419.
34. Axup JY, et al. (2012) Synthesis of site-specific antibody-drug conjugates using unnatural amino acids. *Proc Natl Acad Sci USA* 109(40):16101–16106.
35. Kim CH, et al. (2012) Synthesis of bispecific antibodies using genetically encoded unnatural amino acids. *J Am Chem Soc* 134(24):9918–9921.
36. Cao Y, et al. (2015) Multiformat T-cell-engaging bispecific antibodies targeting human breast cancers. *Angew Chem Int Ed Engl* 54(24):7022–7027.
37. Kim CH, et al. (2013) Bispecific small molecule-antibody conjugate targeting prostate cancer. *Proc Natl Acad Sci USA* 110(44):17796–17801.
38. Long AH, et al. (2015) 4-1BB costimulation ameliorates T cell exhaustion induced by tonic signaling of chimeric antigen receptors. *Nat Med* 21(6):581–590.
39. Haso W, et al. (2013) Anti-CD22-chimeric antigen receptors targeting B-cell precursor acute lymphoblastic leukemia. *Blood* 121(7):1165–1174.
40. Stärck L, Scholz C, Dörken B, Daniel PT (2005) Costimulation by CD137/4-1BB inhibits T cell apoptosis and induces Bcl-xL and c-FLIP(short) via phosphatidylinositol 3-kinase and AKT/protein kinase B. *Eur J Immunol* 35(4):1257–1266.
41. Kalaitsidou M, Kueberuwa G, Schütt A, Gilham DE (2015) CAR T-cell therapy: Toxicity and the relevance of preclinical models. *Immunotherapy* 7(5):487–497.
42. Kochenderfer JN, Yu Z, Frasheri D, Restifo NP, Rosenberg SA (2010) Adoptive transfer of syngeneic T cells transduced with a chimeric antigen receptor that recognizes murine CD19 can eradicate lymphoma and normal B cells. *Blood* 116(19):3875–3886.
43. Davila ML, Kloss CC, Gunset G, Sadelain M (2013) CD19 CAR-targeted T cells induce long-term remission and B Cell aplasia in an immunocompetent mouse model of B cell acute lymphoblastic leukemia. *PLoS One* 8(4):e61338.
44. Hudecek M, et al. (2015) The nonsignaling extracellular spacer domain of chimeric antigen receptors is decisive for in vivo antitumor activity. *Cancer Immunol Res* 3(2): 125–135.
45. Qin H, et al. (2015) Eradication of B-ALL using chimeric antigen receptor-expressing T cells targeting the TSLPR oncoprotein. *Blood* 126(5):629–639.
46. Bluemel C, et al. (2010) Epitope distance to the target cell membrane and antigen size determine the potency of T cell-mediated lysis by BiTE antibodies specific for a large melanoma surface antigen. *Cancer Immunol Immunother* 59(8):1197–1209.
47. Long AH, Haso WM, Orentas RJ (2013) Lessons learned from a highly-active CD22-specific chimeric antigen receptor. *OncoImmunology* 2(4):e23621.
48. Wang R, Natarajan K, Margulies DH (2009) Structural basis of the CD8 alpha beta/MHC class I interaction: Focused recognition orients CD8 beta to a T cell proximal position. *J Immunol* 183(4):2554–2564.
49. Rodgers D, et al. (2015) Switch-mediated activation and retargeting of CAR-T cells for B-cell malignancies. *Proc Natl Acad Sci USA* 113:E459–E468.
50. Wang QS, et al. (2015) Treatment of CD33-directed chimeric antigen receptor-modified T cells in one patient with relapsed and refractory acute myeloid leukemia. *Mol Ther* 23(1):184–191.